J Mater Sci (2010) 45:1540–1546
DOI 10.1007/s10853-009-4121-4

Influence of layer microstructure on the corrosion behavior of plasma nitrided cold work tool steel

Dong-Cherng Wen

Received: 22 September 2009 / Accepted: 9 November 2009 / Published online: 29 December 2009

Abstract The influence of layer microstructure on the corrosion behavior of plasma nitrided cold work tool steel, of commercial name "DC53", in 3.5% NaCl solution is reported. The specimens were nitrided at 520 °C for different treatment times using a constant [$N_2 + H_2$] gaseous mixture by a DC-pulsed plasma system. The microstructure of the nitrided layers was investigated by optical microscopy and X-ray diffraction. The corrosion behavior was evaluated by potentiodynamic polarization experiments. The plasma nitriding process considerably improves the corrosion resistance of material in NaCl environment as compared to the unnitrided DC53 steel. The modified surface layer consisting mainly of ε-nitride ($Fe_{2-3}N$) and a small amount of γ'-nitride (Fe_4N) confers this outstanding behavior. The corrosion resistance dependence on specific nitriding processes is reported and the role of the ε-nitride is discussed. In particular, the correlation of pitting current density, density of pits, and volume fraction of ε-nitride with nitriding time is analyzed. The results denote that the most important parameter for controlling the corrosion resistance of the material is the volume fraction of ε-nitride and the nitrided layer thickness. It is expected that a nitrided layer would be thicker and rich in ε-nitride phase to achieve a high corrosion resistance.

D.-C. Wen (✉)
Department of Mechanical Engineering, China University of Science and Technology, No. 245, Sec. 3, Academia Rd., Nangang District, Taipei City 11581, Taiwan, ROC
e-mail: dcwen@cc.chit.edu.tw

Introduction

Cold work tool steels are widely used in the metal-forming and die-making industries and in many other fields due to their high hardness. One such is DC53 cold work tool steel, a tool material developed by Daido Steel, Japan. This new material is intended to replace JIS SKD11 in use for general purposes [1]. In applications such as dies or tools, the long-service life of tools and the demands for materials with properties such as dimensional stability, superior mechanical strength, and high corrosion resistance are critical to the effective and efficient usage of tools. With such stringent requirements, many surface treatments, such as nitriding [2], laser surface alloying [3], and deposit film [4–6], may provide a solution for improvement by forming a thin, hard case with suitable corrosion and wear resistance on the surface. Besides, some investigations used the heat treatment and powder metallurgy processes to improve the corrosion resistance of the material [7–9].

Plasma nitriding has been receiving a great attention due to its reduced distortion and environment-friendly process. This technique is a thermochemical process in which a gas mixture of N_2 and H_2 is introduced into the chamber. Under such conditions, in the structure of the nitrided layers, the top nitrided layer, known as the compound layer, is composed mainly of ε-nitride ($Fe_{2-3}N$) and γ'-nitride (Fe_4N) as well as nitrides with alloying elements. The layer beneath the compound layer is known as the so-called diffusion layer, which consists mainly of interstitial atoms in solid solution and fine, coherent nitride precipitates when the solubility limit is reached. The thickness and compositions of these layers are functions of treatment condition and composition of the base material [10–13]. The ε-nitride shows better corrosion resistance when compared with γ'-nitride because of its crystalline

structure and higher nitrogen content [14]. Another investigation reported that γ'-nitride formed after iron nitriding in the surface layer is relatively stable in corrosive medium [15]. The corrosion resistance of the nitrided layer, thus, depends on the type of nitride formed in the nitrided layer. Because DC53 cold work tool steel is a new tool steel; for a deeper understanding, the effects of plasma nitriding on its microstructures and corrosion behavior are essential, but very little work has been done on these aspects.

In this study, DC53 tool steel was plasma nitrided at 520 °C for 4, 8, and 12 h. The metallurgical structures and corrosion behavior of the surface nitrided layer are evaluated, analyzed, and discussed.

Experimental details

Specimens were made out of DC53 cold work tool steel (C 0.9–1.1, Si 0.3, Mn 0.5, P < 0.03, S < 0.03, Cr 7–9, Mo 0.8–2.2, V 0.3, Fe balanced all, in wt%) and machined to 12.7 × 12.7 × 12.7 mm^3 in size. The specimens were heated at 1010 °C for 1 h, oil quenched, double tempered at 530 °C for 2 h, and air cooled. Prior to the nitriding process, the specimens were polished to the same surface roughness (R_a = 0.04 μm) and cleaned in an ultrasonic bath with acetone. The DC-pulsed plasma nitriding was carried out in a hot wall reactor, from ELTROPULS GmbH [14]. The specimens were sputter cleaned in an atmosphere of 80% Ar + 20% H_2 at about 250 °C for 1 h, to remove the oxide layers formed on their surfaces. They were then plasma nitrided in an atmosphere of 25% N_2 + 75% H_2 at 520 °C for 4, 8, and 12 h, with the chamber pressure maintained at 600 Pa. The plasma nitriding temperature was controlled to an accuracy of ±5 °C, using a photoelectric thermometer. After the nitriding process was completed, the specimens were allowed to cool in the chamber to room temperature in a stream of flowing nitrogen to protect the heated surfaces from oxidation. The parameters used in the experiment are summarized in Table 1.

The microstructures of nitrided layers were observed by an Olympus BHM optical microscope (OM). X-ray diffraction (XRD) investigations of the nitrided layer were carried out using a Shimadzu X-ray diffractometer (LabX XRD-6000) with CuKα radiation and the symmetric Bragg–Brentano attachment geometry. Quantitative analysis was carried out using the normalized relative (integrated) intensity ratio (RIR) method or the matrix flushing method [16].

A potentiostat/galvanostat (EG&G 362) outfitted with analysis software (CorrWare) was utilized to collect electrochemical data in 3.5% NaCl solution. The use of 3.5% NaCl solution was to simulate the aggressive aqueous environment containing chloride ions. A saturated calomel electrode (SCE) was used as a reference with platinum sheet as a counter electrode. In all cases tested, the working areas were 1 cm^2 and carried out at ambient temperature. The electrode potential was raised from −1 to +3.0 V at the scanning rate of 1 mV/s. After the electrochemical tests, the surface morphologies were inspected using a JEOL JSM-5600 scanning electron microscope (SEM) to reveal the severity of corrosion degradation in terms of pit morphology, distribution, and density. At lease three tests were carried out for each specimen type for assessing the reproducibility.

Table 1 Parameters for plasma-nitriding treatments

Parameter	Sputter cleaning	Plasma nitriding
Temperature (°C)	250	520
Voltage (V)	400	600
Current density (mA/cm^2)	0.8	1.2
Total pressure (Pa)	200	600
Time (h)	1	4; 8; 12
Treatment gas (vol)	80% Ar + 20% H_2	25% N_2 + 75% H_2

Results and discussion

Microstructure

Figure 1 shows the microstructure of unnitrited DC53 cold work tool steel. There were many coarse chromium carbide particles dispersed in the tempered martensite matrix. Because, the major amount of Cr in DC53 steel is formed as coarse chromium carbide particles, thus, the corrosion resistance of the unnitrided DC53 steel is very poor. Figure 2 shows the typical cross-sectional images of

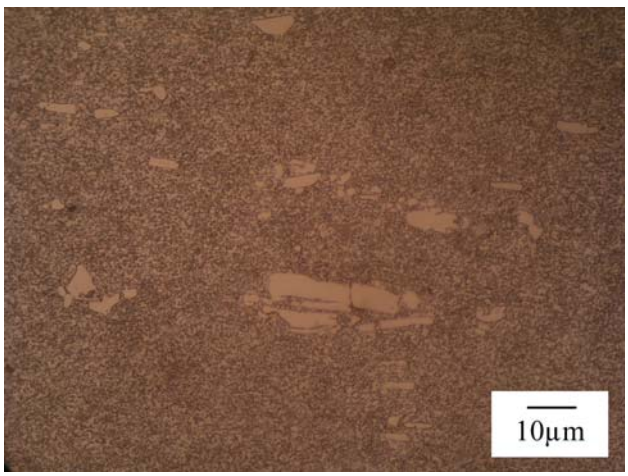

Fig. 1 Microstructure of unnitrited DC53 cold work tool steel (Nital 4%)

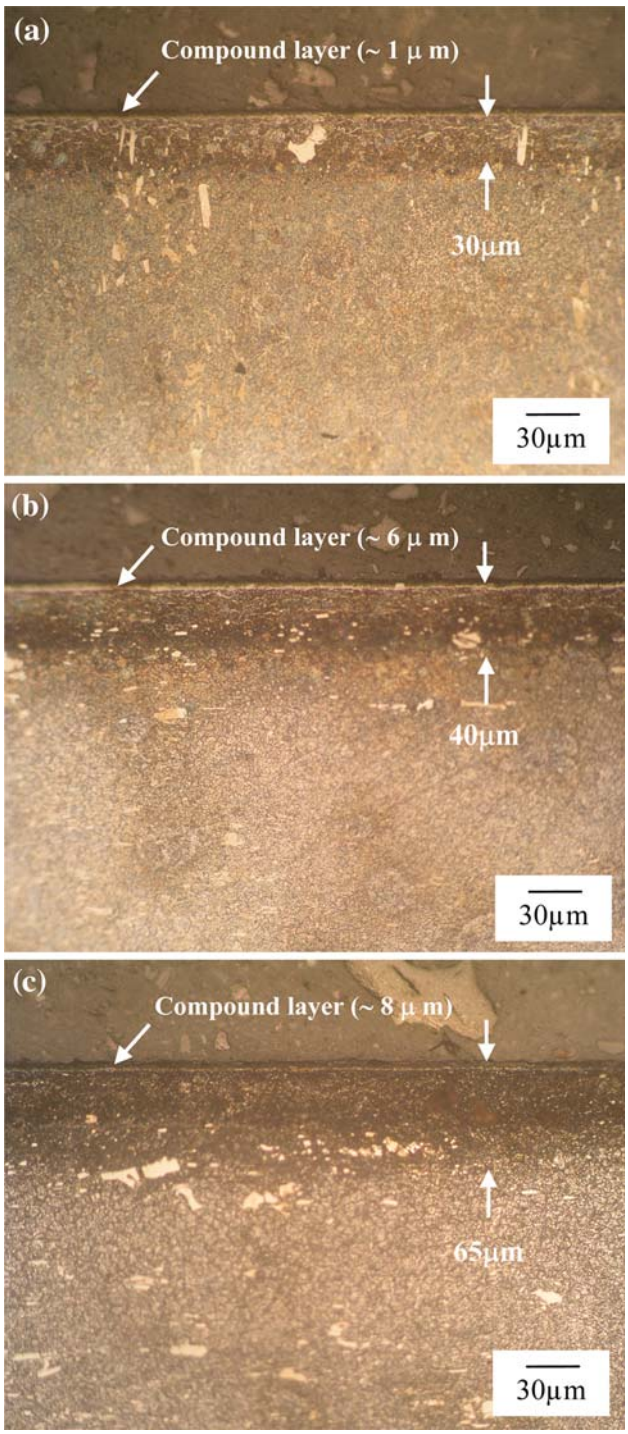

Fig. 2 Optical microscopy image of the specimen nitrided at 520 °C for **a** 4 h, **b** 8 h, and **c** 12 h (Nital 4%)

plasma-nitrided specimen. It consisted of an internal nucleus of tempered martensite and a nitrided layer on the external surface. The nitrided surface consisted of two layers in which a white compound layer and a diffusion layer of nitrogen were clearly observed on the surface and near surface region of all specimens. For lower treatment time, a thin (~1 μm) compound layer is obtained. At intermediate treatment time, the compound layer becomes thicker (~6 μm) than at lower treatment time. At higher treatment time, despite achieving thicker compound layer (~8 μm), it becomes non-porous and dense in nature, as shown in Fig. 3. The depth of diffusion layer also increased with increasing nitriding time.

Figure 4 shows the XRD patterns obtained from the surface of unnitrided and plasma-nitrided specimens. These patterns show the effects of nitriding time on the nitride formation. The iron nitrides on the outermost surface of all nitrided specimens were identified to be ε-nitride ($Fe_{2-3}N$) and γ′-nitride (Fe_4N), and the major phase is ε-nitride. Additionally, some CrN carbides would be precipitated at

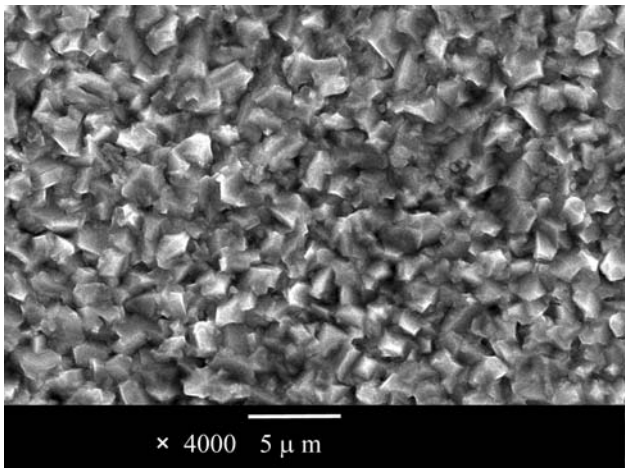

Fig. 3 SEM surface morphology of the specimen nitrided at 520 °C for 12 h

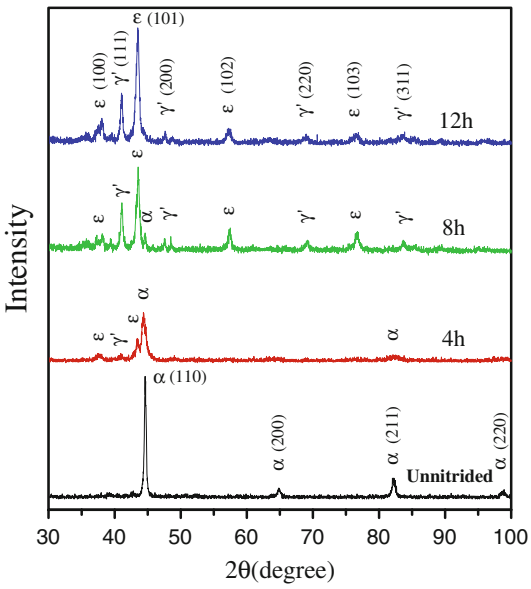

Fig. 4 XRD diffraction patterns of DC53 cold work tool steel

the working temperature of 520 °C and the CrN peaks are very close and also under iron nitride peaks and then it is very difficult to separate from iron nitrides in the spectra. However, the formation of CrN carbides in detriment of the corrosion resistance is not noticeable because the corrosion resistance of unnitrided DC53 steel is poor and the iron nitrides formed after nitriding in improving the corrosion resistance is significant. Thereby, the peaks of CrN carbides and their deterioration in corrosion resistance are negligible.

For the specimen nitrided at 520 °C for 4 h, the nitrided layer consists mainly of α-Fe; some weak peaks of ε- and γ′-nitrides have also been observed. This is consistent with the fact that very thin compound layer has been observed above the diffusion layer. The microstructure of the diffusion layer is composed of fine alloy carbides dispersed in α-Fe(N) matrix. CuKα X-ray could penetrate this thin layer, therefore, the peaks corresponding to α-Fe phase are revealed. The XRD patterns of the 8 and 12 h nitrided specimens indicate that the compound layer consists chiefly of ε-nitride with a small amount of γ′-nitride. Due to the formation of dense and thick compound layer on the surface of the 12-h nitrided specimen, the peaks of α-Fe phase is almost disappeared. It is clearly that the intensity of the nitrided peaks increases with increasing nitriding time. This can be ascribed to the nitrogen diffusion length during the plasma process.

Optical microscopy and XRD analysis show that the microstructure of the nitrided case is time depended. The intensity of the α-Fe peaks progressively decreased, and the intensity of the nitride peaks progressively increased with increasing in nitriding time, indicating an increase in volume fraction of the nitride phase at the expense of parent α-Fe.

Corrosion behavior

Figure 5 shows the potentiodynamic polarization curves of the studied specimens. The summary of corrosion parameters obtained from the potentiodynamic polarization diagram (Fig. 5) is display in Table 2. A corrosion current density of 1 mA/cm^2 is equal to a weight loss of 1.04 mg/cm^2/h according to Faraday's law, assuming a density of 7.8 g/cm^3 and the atomic weight of iron as 55.85 for DC53 tool steel. It was seen that the unnitrided specimen did not have an evident passivation region and suffered progressive dissolution, and the corrosion potential was −0.45 V (SCE), indicating that the DC53 steel is relatively easily corroded in NaCl solution. This is consistent with the fact that the typical appearance of general corrosion was clearly observed on the corroded surface (Fig. 6a). A high corrosion current density (1.83×10^{-1} mA/cm^2) and a high corrosion rate (0.19 mg/cm^2/h) thus resulted under the anodic potential. On the other hand, all nitriding processes shifted the corrosion potential in the noble direction and promoted passivation resulting in very low corrosion current density (2.85×10^{-3}–2.25×10^{-4} mA/cm^2) and very high corrosion potential, −0.092 to −0.026 V (SCE). Between the above corrosion potential and around 1.25 V (SCE), there appeared an evident passivation region. At 1.25 V (SCE), the corresponding current density is 1.06×10^{-1}, 5.72×10^{-2}, and 9.07×10^{-3} mA/cm^2 for the treated specimens at 4, 8, and 12 h, respectively. Above 1.25 V, the nitrided protecting layer broke up, increasing the corrosion current density, and an important pitting process takes place. In this case, general corrosion was not found, but also only small and shallow corroded holes were formed (Fig. 6b). Therefore, the nitrided specimens showed very low corrosion rate (0.003–0.0005 mg/cm^2/h). It was observed that with an increase in nitriding time, the corrosion potential slightly increased (∼0 V), whereas the corrosion and pitting current densities decreased (Table 2). The enhanced corrosion resistance was attributed to the presence of a dense nitride layer rich in ε-nitride phase on the surface. Because nitride is a noble phase, formation of

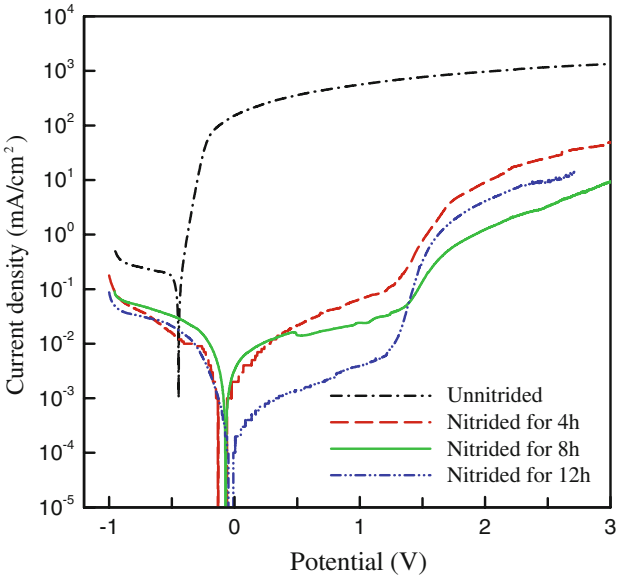

Fig. 5 Polarization curves of DC53 cold work tool steel in 3.5% NaCl solution

Table 2 Corrosion parameters of DC53 cold work tool steel

Treating time (h)	Corrosion potential (V)	Corrosion current density (mA/cm^2)	Corrosion rate (mg/cm^2 h)	Pitting current density (mA/cm^2)
Unnitride	−0.45	1.83×10^{-1}	0.19	–
4	−0.092	2.85×10^{-3}	0.003	1.06×10^{-1}
8	−0.071	1.02×10^{-3}	0.001	5.72×10^{-2}
12	−0.026	2.25×10^{-4}	0.0005	9.07×10^{-3}

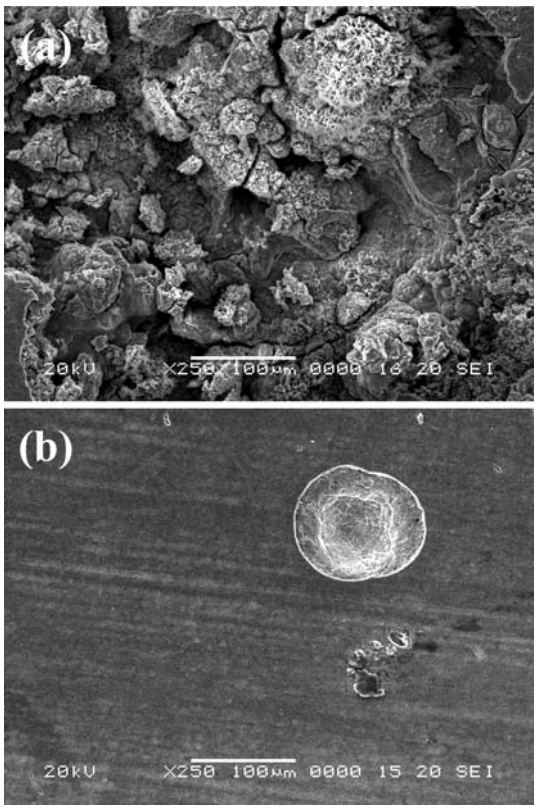

Fig. 6 Surface appearance of the corroded specimens: **a** unnitrided DC53, **b** nitrided for 12 h

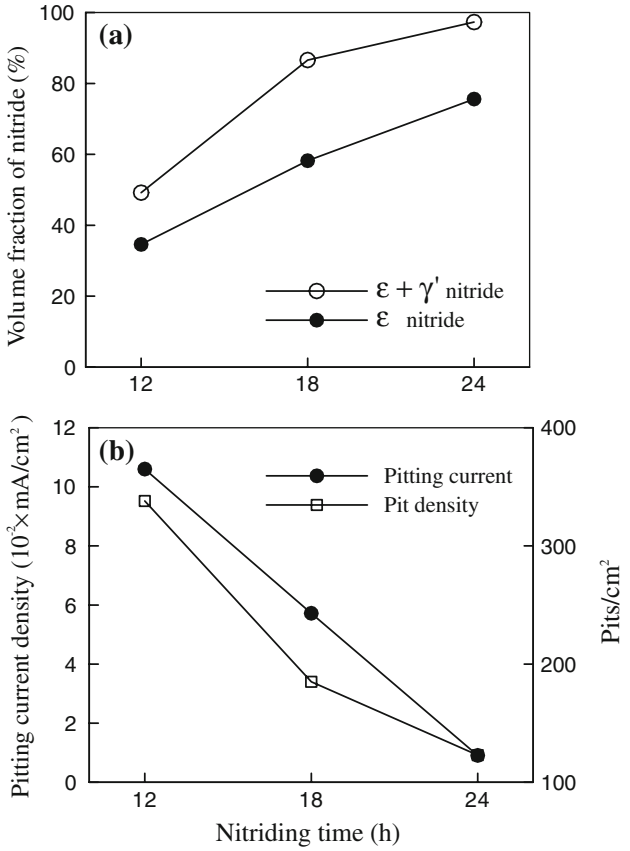

Fig. 7 **a** The amount of nitride measured by quantitative analysis from XRD patterns. **b** Pitting current density and density of pits for nitrided specimens

more nitride helps to protect the surface from corrosion attack, and for this reason, with an increase in nitriding time, corrosion resistance improves. This result agrees quite well with the plasma nitriding study [17] which showed that the nitrided layer with the ε-phase has excellent corrosion resistance.

The volume fraction of ε-nitride obtained from the XRD patterns by using the RIR method, density of pits and pitting current density of the nitrided layers are analyzed as a function of treatment time (Fig. 7). The volume fraction of ε-nitride and total nitrides increased with increasing nitriding time (Fig. 7a). Although the amount of γ′-nitride also increased, the increase in total nitrides was primarily ascribed to the ε-nitride. Because the amount of ε-nitride was much larger than that of γ′-nitride for all nitrided specimens ($\varepsilon/\gamma' > 2$).

The 4-h nitrided specimen showed a relative higher pitting current density (1.06×10^{-1} mA/cm^2). After the test, the corroded surface showed the highest pits (821/cm^2, measured by image analysis of the SEM micrograph) as shown in Fig. 8a. The high density of pits formed during the corrosion tests could be due to a very large number of sites in which local breakdown of the passivity can easily occur. The observed corrosion behavior could be ascribed to the fact that the amount of ε-nitride (37.8%) was lower in 4 h nitrided surface layer in comparison with the other nitrided specimens.

Specimen nitrided for 8 h showed a medium pitting current density (5.72×10^{-2} mA/cm^2). After linear polarization, the corroded surface showed the presence of smaller (mean pits diameter: ∼198 μm) and fewer pits (493/cm^2) as shown in Fig. 8b. This behavior could be attributed to the moderate amount of ε-nitride (55.7%) formed on the nitrided layer.

In the 12-h nitrided specimen, the pitting current density showed a significant reduction (9.07×10^{-3} mA/cm^2) in comparison with the other nitrided specimens. After the linear polarization, the specimen showed the lowest pits (356/cm^2) on the corroded surface as shown in Fig. 8c. This indicated very small number of sites in which the local breakdown of passivity occurred during the corrosion tests. This behavior was due to a dense protective nitrided layer with high amount of ε-nitride (69.1%) formed on the surface.

The corrosion mechanism in austenitic stainless steel (ASS) and martensitic stainless steel (MSS) has been reported [18, 19]. In ASS, the CrN precipitation is the main factor for the degradation of corrosion resistance compared

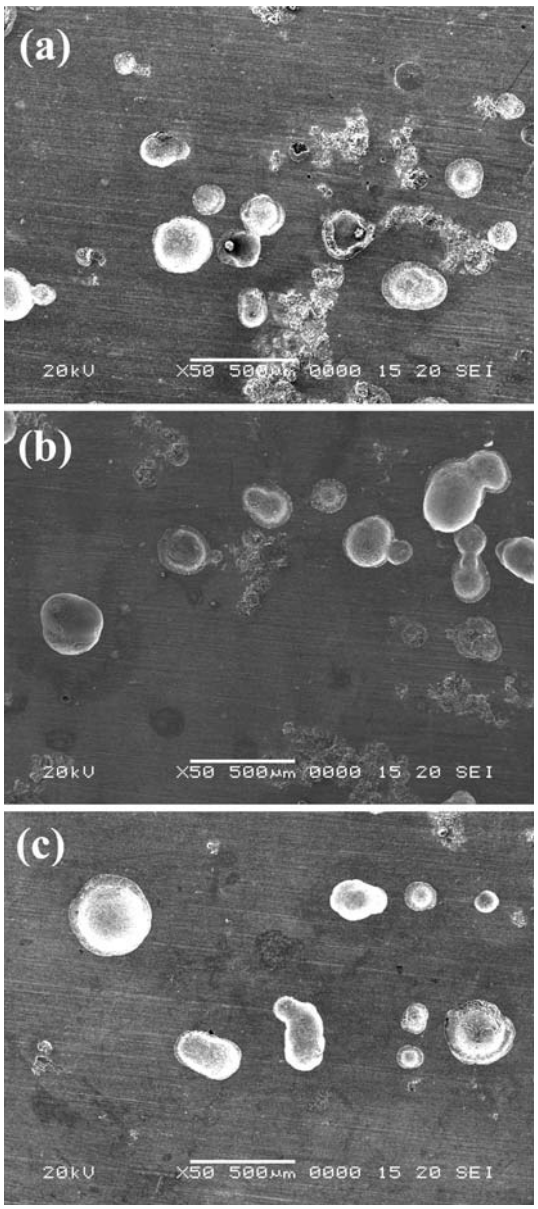

Fig. 8 Surface appearance of the corroded specimens showing the density of pits: nitrided for **a** 4 h, **b** 8 h, and **c** 12 h

to the untreated material. However, in MSS, the plasma-nitriding treatment improves the corrosion resistance, even after CrN precipitation, compared to the untreated material. In our case, the quantity of CrN precipitation is low. Therefore, the most important parameter for controlling the corrosion resistance of the nitrided specimen is the volume fraction of ε-nitride and the thickness of the nitrided layer. As shown in Fig. 7, the volume fraction of ε-nitride increased with increasing nitriding time while the pitting current density and the density of pits followed the opposite trend and ultimately showed drastic reduction in corrosion rate after plasma nitriding. These results confirm the increase in corrosion resistance by coverage of nitride phase. A thicker and dense-nitrided layer would always enhance the corrosion resistance [20]. Furthermore, improvement in corrosion resistance is found to be directly related to the increase in the amount of ε-nitride at the surface; it agrees with that the most important factor for controlling the corrosion resistance of the nitrided specimens is the amount of ε-nitride.

Conclusions

The influence of microstructure on the corrosion behavior of plasma-nitrided cold work tool steel (DC53) was studied. The volume fraction of ε-nitride, density of pits, and pitting current density of the nitrided layers are analyzed as a function of treatment time. It has been confirmed that the corrosion resistance of the material depended on the specific nitriding processes. For short nitriding time, the formed thin nitrided layer with lower amount of ε-nitride shows relatively poor corrosion resistance. At intermediate nitriding time, a thicker nitrided layer with the moderate amount of ε-nitride formed on the nitrided layer improves the corrosion resistance of the material. For long nitriding time, a most thick and dense protective nitrided layer with high amount of ε-nitride is formed on the surface, guaranteeing good corrosion resistance. These results confirm that the most important parameter for controlling the corrosion resistance of the material is the volume fraction of ε-nitride and the thickness of the nitrided layer. It is expected that a nitrided layer would be thicker and rich in ε-nitride phase to achieve a high corrosion resistance.

References

1. http://www.daido.co.jp/english/products/tool/coldwork_properties.html. Accessed 15 July 2009
2. Silva LLG, Ueda M, Mello CB, Codaro EN, Lepienski CM (2008) J Mater Sci 43:5989. doi:10.1007/s10853-008-2768-x
3. Gemelli E, Gallerie A, Kopp FCT, Camargo NHA (2005) J Mater Sci 40:5649. doi:10.1007/s10853-005-1538-2
4. Lunarska E, Michalski J (1995) J Mater Sci 30:4125. doi:10.1007/BF00360719
5. Batory D, Blaszczyk T, Clapa M, Mitura S (2008) J Mater Sci 43:3385. doi:10.1007/s10853-007-2393-0
6. Mao ZP, Ma J, Wang J, Sun B (2009) J Mater Sci 44:3265. doi:10.1007/s10853-009-3438-3
7. Sundararajan G, Phani PS, Jyothirmayi A, Gundakaram RC (2009) J Mater Sci 44:2320. doi:10.1007/s10853-008-3200-2
8. Calliari I, Brunelli K, Zanellato M, Ramous E, Bertelli R (2009) J Mater Sci 44:3764. doi:10.1007/s10853-009-3505-9
9. Balaji S, Upadhyaya A (2009) J Mater Sci 44:2310. doi:10.1007/s10853-008-3020-4
10. Collins GA, Hutchings R, Tendys J (1991) Mater Sci Eng A 139:171
11. Li S, Manory RR (1999) J Mater Sci 34:1045. doi:10.1023/A:1004548112547

12. Shetty K, Kumar S, Rao PR (2009) Surf Coat Technol 203:1520
13. Wang J, Xiong J, Peng Q, Fan H, Wang Y, Li G, Shen B (2009) Mater Charact 60:197
14. Oliveira SD, Tschiptschin AP, Pinedo CE (2007) Mater Des 28:1714
15. Fu RKY, Tang DL, Wan GJ, Chu PK (2007) Surf Coat Technol 201:4879
16. Chung FH (1974) J Appl Crystallogr 7:519
17. Wen DC (2009) Surf Coat Technol 204:511
18. Li CX, Bell T (2006) Corros Sci 48:2036
19. Rao VS, Singhal LK (2009) J Mater Sci 44:2327. doi:10.1007/s10853-008-2976-4
20. Ensinger W, Schröer A, Wolf GK (1992) Surf Coat Technol 51:217